

A Comparative Evaluation of Aura-OMI and SKYNET Near-UV Single-scattering Albedo Products

Hiren Jethva^{1,2*}, Omar Torres²

¹Universities Space Research Association, Columbia, MD 21044 USA

²NASA Goddard Space Flight Center, Greenbelt, MD 20771 USA

Mailing Address:

Room#A422, Building#33,

Laboratory of Atmospheric Chemistry & Dynamics

Earth Science Division

NASA Goddard Space Flight Center,

Greenbelt, MD 20771, USA

* **Corresponding Author: Dr. Hiren Jethva**

E-mail: hiren.t.jethva@nasa.gov

24 **ABSTRACT**

25 The aerosol single-scattering albedo (SSA) retrieved by the near-UV algorithm applied to the
26 Aura/Ozone Monitoring Instrument (OMI) measurements (OMAERUV) is compared with an
27 independent inversion product derived from the sky radiometer network SKYNET—a ground-
28 based radiation observation network with sites in Asia and Europe. The present work continues
29 previous efforts to evaluate the consistency between the retrieved SSA from satellite and
30 ground sensors. The automated spectral measurements of direct downwelling solar flux and sky
31 radiances made by SKYNET Sun-sky radiometer are used as input to an inversion algorithm that
32 derives spectral aerosol optical depth (AOD) and single-scattering albedo (SSA) in the near-UV
33 to near-IR spectral range. The availability of SKYNET SSA measurements in the ultraviolet region
34 of the spectrum allows, for the first time, a direct comparison with OMI SSA retrievals
35 eliminating the need of extrapolating the satellite retrievals to the visible wavelengths as the
36 case in the evaluation against the Aerosol Robotic Network (AERONET). An analysis of the
37 collocated retrievals from over 25 SKYNET sites reveals that about 61% (84%) of OMI-SKYNET
38 matchups agree within the absolute difference of ± 0.03 (± 0.05) for carbonaceous aerosols, 50%
39 (72%) for dust aerosols, and 45% (75%) for urban-industrial aerosol types. Regionally, the
40 agreement between the two inversion products is robust over several sites in Japan influenced
41 by carbonaceous and urban-industrial aerosols; at the biomass burning site *Phimai* in Thailand,
42 and polluted urban site in *New Delhi*, India. The collocated dataset yields fewer matchups
43 identified as dust aerosols mostly over the site *Dunhuang* with more than half of the matchup
44 points confined to within ± 0.03 limits. Altogether, the OMI-SKYNET retrievals agree within
45 ± 0.03 when SKYNET AOD (388 or 400 nm) is larger than 0.5 and OMI UV Aerosol Index larger
46 than 0.2. The remaining uncertainties in both inversion products can be attributed to specific
47 assumptions made in the retrieval algorithms, i.e., the uncertain calibration constant,
48 assumption of spectral surface albedo and particle shape, and sub-pixel cloud contamination.
49 The assumption of fixed and spectrally neutral surface albedo (0.1) in the SKYNET inversion
50 appears to be unrealistic, leading to underestimated SSA, especially under lower aerosol load
51 conditions. At higher AOD values for carbonaceous and dust aerosols, however, retrieved SSA

52 values by the two independent inversion methods are generally consistent in spite of the
53 differences in retrieval approaches.

54 **1 INTRODUCTION**

55 Satellite-based remote sensing of aerosols has become an essential tool to detect, quantify, and
56 routinely monitor the aerosol optical and size properties over the globe. An accurate
57 representation of aerosols in the climate models is an essential requirement for reducing the
58 uncertainty in aerosol-related impact on the Earth's radiation balance (direct and semi-direct
59 effects) and cloud microphysics (indirect effect) (*IPCC, 2013*). The fundamental aerosol
60 parameters determining the strength and sign of the radiative forcing are the aerosol optical
61 depth (AOD) and single-scattering albedo (SSA) in addition to the reflective properties of the
62 underlying surface. While the columnar AOD represents the total extinction (scattering and
63 absorption) resulting from the interactions with solar radiation, SSA describes the relative
64 strength of scattering to the total extinction. Together, both AOD and SSA determine the
65 magnitude and sign of the aerosol radiative forcing at the top-of-atmosphere. For example, a
66 decrease in SSA from 0.9 to 0.8 can often change the sign of radiative forcing from negative
67 (cooling) to positive (warming) that also depends on the albedo of the underlying surface and
68 the altitude of the aerosols (*Hansen et al., 1997*). Thus, an accurate estimate of both quantities
69 is a prime requirement for reliable estimates of the net effect of atmospheric aerosols
70 produced with the anthropogenic as well as natural activities.

71
72 Launched in July 2004, the Ozone Monitoring Instrument (OMI) onboard NASA's Aura satellite
73 has produced more than a decade long global record of observations of reflected radiation
74 from Earth in the 270–500 nm wavelength range of the spectrum on a daily basis. OMI scans
75 the entire Earth in 14 to 15 orbits with its cross-track swath of ~2600 km at ground level at a
76 nadir ground pixel spatial resolution of $13 \times 24 \text{ km}^2$. OMI observations of the top-of-
77 atmosphere reflected light at 354 and 388 nm wavelengths are used to derive the UV aerosol
78 index (UVAI) as well as the AOD and SSA using the OMAERUV algorithm that takes advantage of
79 the well-known sensitivity to the aerosol absorption in the UV spectral region (*Torres et al.,*
80 *1998*). While a general description of the OMAERUV algorithm is presented in *Torres et al.*
81 (*2007*), the recent algorithmic upgrades are documented in *Torres et al. (2013, 2018)*. The most

82 important changes applied in the latest OMAERUV algorithm upgrade includes: 1) use of new
83 carbonaceous aerosol models that account for the presence of organics in the carbonaceous
84 aerosols by assuming wavelength-dependent imaginary part of the refractive index (*Jethva and*
85 *Torres, 2011*), 2) an implementation of robust scheme to identify aerosol type (smoke, dust,
86 urban/industrial) that combinedly uses the information on carbon monoxide (CO) observations
87 from the Atmospheric Infrared Sounder (AIRS) and UVAI from OMI (*Torres et al., 2013*), 3) use
88 of the aerosol height climatology dataset derived from the Cloud-Aerosol Lidar with Orthogonal
89 Polarization (CALIOP) lidar-based measurements of the vertical profiles of aerosol for the
90 carbonaceous and dust aerosols (*Torres et al., 2013*), and 4) better treatment of dust particles
91 assuming realistic spheroidal shape distribution (*Torres et al., 2018*). Additionally, the upgraded
92 OMAERUV algorithm has adopted a new method to calculate UVAI, which now accounts for the
93 angular scattering effects of clouds and significantly reduces a scan angle related asymmetry in
94 UVAI in cloudy scenes (*Torres et al., 2018*).

95

96 The present work continues previous efforts to evaluate the consistency between ground-
97 based SSA measurements and satellite retrievals from near UV observations. On the first
98 attempt to intercompare space-based and surface near UV SSA measurements, Earth Probe
99 TOMS retrievals were compared to AERONET observations acquired during the SAFARI 2000
100 field campaign (*Torres et al., 2005*). The OMAERUV near-UV aerosol product of AOD and SSA
101 has been continually assessed and validated against the ground-based measurements acquired
102 from the globally distributed Aerosol Robotic Network-AERONET (*Torres et al., 2007; Ahn et al.,*
103 *2008; Jethva and Torres, 2011; Ahn et al., 2014; Jethva et al., 2014*). While the OMAERUV AOD
104 product was directly validated against the AERONET measurements made in the near-UV (340-
105 380 nm), as carried out in *Ahn et al. (2014)*, the SSA retrievals have been evaluated by
106 comparison with the AERONET ground inversion product (*Jethva et al., 2014*). The latter
107 analysis required OMI retrievals of SSA to be extrapolated to the shortest visible wavelength of
108 440 nm of AERONET inversion product to make the comparison possible. Such adjustment in
109 the wavelength of retrievals can introduce uncertainty in the comparison arising from the
110 inaccuracy of the spectral dependence of absorption assumed in the wavelength conversion.

111
112 A direct comparison of the column-integrated SSA at 388 nm retrieved from OMI requires
113 equivalent ground-based columnar retrievals in the near-UV region. The international network
114 of scanning sun-sky radiometers (SKYNET) fulfills this requirement as it performs the direct Sun
115 and sky measurements in the near-UV (340-380 nm) as well as visible/near-IR (400-1020 nm)
116 regions of the spectrum and derives spectral AOD and SSA. Taking advantage of the availability
117 of ground-based SSA inversions in the near-UV from SKYNET, we inter-compare the OMI and
118 SKYNET SSA products at several SKYNET sites in Asia and Europe. Since both retrieval
119 approaches are based on inversion algorithms that rely on assumptions, the resulting level of
120 agreement can only be interpreted as a measure of consistency (or lack thereof) in the
121 measurement of the same physical parameter by fundamentally different remote sensing
122 approaches.

123
124 The paper is organized as follows: Section 2 describes the satellite and ground-based data sets
125 assessed in this analysis along with the collocation methodology; the results of OMI-SKYNET
126 SSA comparison over individual sites, combinedly for each aerosol type, and diagnosis of
127 differences between them are presented in section 3; the possible sources of uncertainty in
128 both inversion products are discussed in section 4; the paper is summarized and concluded in
129 section 5.

130

131 **2 DATASETS**

132 **2.1 THE OMI-OMAERUV AEROSOL PRODUCT**

133 The entire record of OMI observations (October 2004 to present) has been reprocessed
134 recently with the refined OMAERUV algorithm (PGEVersion V1.8.9.1) to derive a comprehensive
135 aerosol product that includes the retrievals of UV Aerosol Index (UVAI), AOD, SSA, and AAOD
136 (388 nm) at a pixel resolution of 13 x 24 km² at nadir viewing geometry. The retrieved

137 parameters are also reported at 354 nm and 500 nm wavelengths following the spectral
138 dependence of aerosols assumed in the chosen model. The data set is available in the HDF-
139 EOS5 format and can be obtained at no cost from NASA Goddard Earth Sciences (GES)-Data and
140 Information Services Center (DISC) server at <http://daac.gsfc.nasa.gov/>. The recent upgrade has
141 been documented in detail in the work of *Jethva and Torres (2011)*, *Torres et al. (2013, 2018)*
142 and *Ahn et al. (2014)*. Here, we use the OMAERUV Level 2 Collection 003 (V1.8.9.1) aerosol
143 product processed in July 2017. The expected uncertainty limits in the OMAERUV SSA retrievals
144 are determined to be ± 0.03 and ± 0.05 , based on its comparison with AERONET SSA inversion
145 and sensitivity analysis carried out during the development of the OMAERUV algorithm (*Torres*
146 *et al., 2007*). Following an early evaluation of OMI aerosol product for a handful of sites, *Jethva*
147 *et al. (2014)* conducted a global evaluation of SSA product and also carried out a detailed
148 uncertainty test considering different sources of errors, such as aerosol model, surface albedo,
149 and aerosol layer height. The results of the sensitivity analysis further confirmed the
150 uncertainty budget estimated earlier during the early development of the OMAERUV algorithm.
151 However, note that the errors could attain larger magnitudes when algorithmic assumptions
152 are far off from the real atmospheric conditions.

153

154 Post-2007, the OMI observations have been affected by a possible external obstruction that
155 perturbs both the measured solar flux and Earth radiance. This obstruction affecting the quality
156 of radiance at all wavelengths for a particular viewing direction is referred to as “row anomaly”
157 (RA) since the viewing geometry is associated with the row numbers on the charge-coupled
158 device detectors. The RA issue was detected first time in mid-2007 with a couple of rows which
159 during the later period of operation expanded to other rows in 2008 and later. At present,
160 about half of the total 60 rows across the track are identified and flagged as row anomaly
161 affected positions for which no physical retrievals are performed (*Schenkeveld et al., 2017*). The
162 details about this issue can be found at
163 <http://www.knmi.nl/omi/research/product/rowanomaly-background.php>. The RA has
164 significantly affected the sampling during post-2008 OMI measurements, where row anomaly
165 flags blanket about half of the OMI swath. As a result, the availability of the number of

166 retrievals since 2009 over a particular site is reduced. Therefore, the OMI-SKYNET matchups are
167 also expected to be lower during the row anomaly affected period. The OMAERUV algorithm
168 assigns quality flags to each pixel which carries information on the quality of the retrieval
169 depending upon the observed condition. We used aerosol retrievals free of RA and flagged as
170 quality flag '0', which are considered best in accuracy due to higher confidence in detecting
171 aerosols in a scene with minimal cloud contamination.

172 **2.2 THE SKYNET AEROSOL INVERSION PRODUCT**

173 The SKYNET is an international network of scanning sun-sky radiometers (manufactured by
174 *Prede Co. Ltd.*, Japan) performing routine and long-term measurements of direct and diffuse
175 solar radiations at several wavelengths spanning UV (340 and 380 nm), visible (400, 500, 675
176 nm), near-IR region (875, 1020 nm), and in shortwave-IR (1627 nm and 2200 nm) of the
177 spectrum. The automated measurements of direct and diffuse solar radiations are used to
178 measure spectral AOD and retrieve SSA and other aerosol optical-microphysical properties
179 (volume size distribution, refractive index, phase function, and asymmetry parameter) at the
180 same standard wavelengths of AOD following an inversion algorithm packaged in the
181 *SKYRAD.pack* software (*Nakajima et al.*, 1996; *Hashimoto et al.*, 2012). Cloudy observations are
182 screened using the Cloud Screening Sky Radiometer code (*Khatri and Takamura*, 2009).

183

184 The SKYNET radiometers come in two flavors, model POM-01 and model POM-02. The POM-01
185 instrument carries a total of five wavelength filters covering visible to near-IR (400-1020 nm),
186 whereas POM-02 instrument has two additional filters in the UV region (340 and 380 nm) along
187 with the other filters in the visible to shortwave-IR (including 1627 nm and 2200 nm) part of the
188 spectrum. The calibration of each SKYNET radiometer is performed on-site on a monthly basis
189 using the improved Langley method (*Nakajima et al.*, 1996; *Campanelli et al.*, 2004, 2007).
190 Occasionally, the inter-calibration of radiometers is carried out against the master instrument
191 well-calibrated using the Langley method on a high mountain site, e.g., Mauna Loa. The SKYNET
192 radiometers are also inter-compared with AERONET Cimel Sunphotometers and precision filter

193 radiometers at three observation sites, i.e., *Chiba University, Valencia (Estelles et al., 2016), and*
194 *Rome (Campanelli et al., 2018).*

195

196 Studies in the past have compared AODs (*Estellés et al., 2012a*) and SSAs (*Estellés et al., 2012b*)
197 measured/retrieved from SKYNET and AERONET and shown that AODs are well-correlated and
198 in good agreement, but the SKYNET SSAs are found to be higher than those of AERONET (*Che et*
199 *al., 2008; Hashimoto et al., 2012*). *Khatri et al. (2016)* further pinpoints the factors, such as
200 quality of input data attributed to different calibration and observation protocols, different
201 quality assurance criteria, the calibration constant for sky radiances, differences in measured
202 AOD, and surface albedo, responsible for the inconsistent aerosol SSA between AERONET and
203 SKYNET using observations from the four representative sites, i.e., Chiba (Japan), Pune (India),
204 Valencia (Spain), and Seoul (South Korea). More discussion on the sources of uncertainties is
205 presented in section 4.

206

207 In this study, we include the SKYNET data acquired over a total of 25 sites distributed mostly
208 across Asia and a few in Europe. The dataset is freely accessible from the data portal of the
209 Center for Environmental Remote Sensing (CERes), Chiba University, Japan
210 (<http://atmos3.cr.chiba-u.jp/skyenet/data.html>). Figure 1 shows the geographic distribution of
211 selected sites, whereas Table 1 lists the geo-coordinates of these sites with the associated
212 sensor type (POM-01 or POM-02) and data periods. The SKYNET aerosol product is derived
213 using two different Skyrad packs: version 4.2 and version 5, the differences of which are
214 explained in *Hashimoto et al. (2012)*. In this study, we use the SKYNET Level 2 product retrieved
215 using version 5 of Skyrad pack. SKYNET retrievals assigned with cloud flag '0' are included in the
216 analysis since these measurements are believed to be free of cloud contamination considered
217 as higher quality retrievals. A careful examination of the SKYNET inversion dataset revealed
218 some irregularities in the measurements for many sites, such as irregular patterns in the shape
219 of spectral SSAs, identical values of SSA at near-UV and visible wavelengths, and much larger
220 standard deviation (>0.1) in SSA within a few hours. These spurious measurements were
221 excluded from the present analysis.

2.3 THE COLLOCATION OF OMI AND SKYNET MEASUREMENTS

OMI retrievals correspond to a spatial scale of $13 \times 24 \text{ km}^2$ at nadir representing the atmospheric conditions over an area. Unlike the direct measurements of the spectral AOD, which correspond to columnar point measurements, the retrievals made by SKYNET use the sky radiances measured at several discrete angles azimuthally, therefore representing the sky condition observed over a station which is associated with approximately 5 km radius surrounding the Sun photometer site. SKYNET retrieves aerosol optical-microphysical properties, including spectral SSA, under all cloud-free conditions and at all aerosol loadings. It is expected that the inversion of retrieved parameters from sky radiances offers better accuracy at larger solar zenith angles owing to the longer optical path and better aerosol absorption signal (*Dubovik et al., 2000*). These conditions are best satisfied with the measurements made during the early morning and late afternoon hours. On the other hand, Aura/OMI overpasses a station during the afternoon hours with the local equator-crossing time 1:30 P.M. Therefore, the collocation of the measurements was carried out within a time window of $\pm 3 \text{ h}$ around OMI overpass time in order to get sufficient high-quality SKYNET retrievals particularly from early morning/late afternoon measurements. The OMI retrievals of SSA were spatially averaged in a grid area of 0.5° by 0.5° centered at the SKYNET site. Though the spatial averaging area for the OMI retrieval is about 50 km^2 , due to its larger footprint, the actual area intercepted by OMI pixels around SKYNET site is likely to be larger.

241

OMI performs retrieval at 354 nm and 388 nm wavelengths, whereas the SKYNET POM-02 instrument reports SSA at nearby wavelengths of 340, 380, and 400 nm. To compare both SSA products at the same wavelength, SKYNET SSA was linearly interpolated at 388 nm, to match with the wavelength of OMI retrieval, using the measurements at the two nearest wavelengths, i.e., 380 nm and 400 nm. The SKYNET POM-01 instruments don't carry UV wavelength filters, but report the retrievals at the shortest wavelength 400 nm and other visible/near-IR wavelengths. In this case, the OMI retrievals are extrapolated from 388 nm to 400 nm, to match with the wavelength of SKYNET inversion, following the spectral dependence of SSA associated

250 with the chosen aerosol model in the OMI algorithm. It is reasonably fair to assume that the
251 extrapolation of OMI SSA in a narrow window of 12-nm, i.e., from 388 to 400 nm, should not be
252 a major source of uncertainty in comparing SSA from OMI and SKYNET.

253 **3 RESULTS**

254 **3.1 OMI-SKYNET COMPARISON OVER INDIVIDUAL STATIONS**

255 Figure 2 displays the OMAERUV versus SKYNET SSA scatterplots for selected sites in Japan. The
256 comparison was made at 388 nm or 400 nm depending upon the availability of the SKYNET
257 inversion at those wavelengths, i.e., POM-01 or POM-02 sensors. Legends with different colors
258 represent the aerosol type selected by the OMAERUV algorithm for the co-located matchups
259 (N). RMSD is the root-mean-square difference between the two retrievals; Q_0.03 and Q_0.05
260 are the percent of total matchups (N) that fall within the absolute difference of 0.03 and 0.05,
261 respectively; horizontal and vertical lines for each matchup are the standard deviation of
262 temporally and spatially averaged SKYNET and OMI SSAs. The comparison includes OMI-SKYNET
263 matchups with AOD>0.3 (388 or 400 nm) in both measurements simultaneously. The
264 scatterplots reveal a good level of agreement for matchups identified with
265 carbonaceous/smoke aerosols over *Chiba University, Cape Hedo, Fukue, Saga, and Etchujima*
266 with the majority of points confined within the absolute difference of 0.03. The OMI-SKYNET
267 combined dataset is dominated with matchup points identified as the urban/industrial aerosols
268 by the OMAERUV algorithm for which the measured UVAI falls below 0.5 representing lower
269 aerosol loading in the boundary layer with weakly absorbing properties. Under such observed
270 conditions, the uncertainties in both kinds of measurements are prone to be larger due to
271 lower absorption signal relative to the instrumental noise and errors in algorithmic assumptions,
272 such as surface albedo, that could further amplify the overall uncertainty in the retrievals.
273 Despite these inherent uncertainties, an agreement within the difference of ± 0.03 for more
274 than half of the collocated retrievals is encouraging.

275

276 Figure 3 shows the scatterplots of OMI-SKYNET SSA for remaining sites located in South Korea,
277 China, Thailand, India, and Italy. For the site *Seoul* in South Korea, OMI tends to overestimate
278 SSA for a number of matchups assigned with the urban/industrial aerosol type and for a few
279 with the carbonaceous/smoke aerosol type such that about 42% of total matchups are falling
280 within the difference of 0.03. For the *Dunhuang* site located in the desert area of China, a
281 majority of collocated data points were identified as dust aerosol type providing an overall
282 better agreement with 50% and 68% matchups bounded within ± 0.03 and ± 0.05 differences,
283 respectively. The *Phimai* site in Thailand is known to be influenced by the springtime biomass
284 burning activities, where OMI and SKYNET SSAs are found to agree relatively best among all 25
285 sites providing 71% and 91% of the matchups restricted within ± 0.03 and ± 0.05 limits,
286 respectively. The agreement between the two sensors was robust for the carbonaceous/smoke
287 aerosol type followed by the urban/industrial aerosols. Over the megacity of New Delhi in the
288 Indo-Gangetic Plain in India, which is seasonally influenced by the smoke and desert dust
289 aerosols in addition to the local source of urban pollution, the OMI-SKYNET matchups are found
290 to agree within ± 0.03 and ± 0.05 for 52% and 83% of the evaluated data points respectively.
291 Over the *Pune* station located near the western boundary of India and the *Bologna* site in Italy,
292 OMI retrieves higher SSA compared to that of SKYNET yielding 39% and 64%, and 25% and 50%
293 matchups, respectively, within the two uncertainty limits. Table 1 lists the statistical measures
294 of the OMI-SKYNET SSA comparison for all 25 sites. A more detailed description of the different
295 sources of uncertainty is presented in section 4.

296 **3.2 COMPOSITES FOR EACH AEROSOL TYPE**

297 Figure 4 displays the composite scatterplots of OMI versus SKYNET SSA derived by segregating
298 the matchup points for each aerosol type from all 25 sites. The intention here is to evaluate the
299 consistency between the two retrieval methods for each aerosol type separately and
300 understand their relative differences. When identified as the carbonaceous/smoke aerosol type,
301 the OMI-SKYNET matchups reveal relatively best comparison among the three major aerosol
302 types with 61% and 84% data points falling within the absolute difference of 0.03 and 0.05,
303 respectively, and providing the lowest (0.035) root-mean-square-difference between the two

304 retrievals. The collocation procedure yields the lowest number of matchups (N=32) for desert
305 dust aerosol type obtained mostly over the site of *Dunhuang* in China, resulting 50% and 72% of
306 data points within the stated uncertainty limits. Among the three aerosol types, the collocated
307 points assigned with the urban/industrial aerosol type (Figure 4 bottom-left) yield the
308 maximum number of matchups (N=739) with the relatively weakest agreement (RMSD=0.052),
309 where OMI tends to overestimate SSA for a significant number of instances resulting about 45%
310 and 67% data points falling within the two limits of expected uncertainties. When more than
311 one prescribed aerosol types are selected for OMI pixels around the SKYNET stations, the
312 matchups between the two sensors resulted in 59% and 77% retrievals within the uncertainty
313 limits with an RMSD of 0.041—a comparison slightly poorer than ‘smoke-only’ case, but better
314 than ‘dust-only’ and ‘urban/industrial-only’ retrieval cases. Combined, all three distinct aerosol
315 types simultaneously yield the total number of matchups (N=1223) with an RMSD of 0.047
316 between OMI and SKYNET resulting 51% and 72% collocated data points falling within the
317 absolute difference of 0.03 and 0.05 difference, respectively. When the restriction of $AOD > 0.3$
318 is removed from the collocation procedure, allowing all matchups regardless of their respective
319 AOD values, the total number of collocated data points was increased to more than twice
320 (N=2691) albeit with a relatively weaker agreement yielding an RMSD of 0.06 and percent data
321 points within the uncertainty limits reducing to 38% and 59%, respectively.

322

323 **3.3 COMPOSITES FOR VARYING AEROSOL LOADING AND POM-01 VERSUS POM-02**

324 Figure 5 shows the number density plots comparing OMI-SKYNET SSA matchups obtained from
325 all sites combined and for varying aerosol loading conditions. The best set of comparison is
326 achieved under the most restrictive scenario when corresponding OMI-retrieved AOD and UVAI
327 are constrained to >0.3 and >0.5 , respectively, albeit with a significantly reduced number of
328 matchups compared to the other two cases with lesser (middle) or no (left) restrictions. The
329 improved comparison reflected in statistical parameters is a result of avoiding retrievals with
330 lower aerosol loading when both kinds of measurements might be subjected to larger
331 uncertainties due to algorithmic assumptions.

332

333 Figure 6 shows the number density plot comparing SSA between SKYNET and OMI for POM-01
334 and POM-02 sensors separately. Overall, no major difference is noticed in the derived statistics
335 between the two sets of comparison, except that the number of matchups obtained with
336 POM02 sensor is 39% more than those with POM01 sensors, and POM02 dataset offers
337 marginally better comparison (except bias, which is higher with POM02) with OMI SSA
338 retrievals. This analysis indicates that the interpolation of OMI SSA from 388 nm to 400 nm for
339 its comparison with POM01 data isn't a significant source of discrepancy between the two SSA
340 datasets.

341

342 **3.4 DIAGNOSIS OF OMAERUV VERSUS SKYNET SSA**

343 The SKYNET algorithm inverts the spectral sky radiances in conjunction with the direct AOD
344 measurements to retrieve the real and imaginary parts of the refractive index and particle size
345 distribution of cloud-free observations under all aerosol loading conditions. These inversion
346 products are believed to be more stable and accurate at higher aerosol loadings and solar
347 zenith angles due to stronger aerosol absorption signal and longer optical path (*Dubovik et al.*,
348 2000). Similarly, a sensitivity analysis of the two-channel OMAERUV retrievals suggests that the
349 retrieved AOD and SSA are susceptible to the small change in surface albedo at lower aerosol
350 loading (*Jethva et al.*, 2014). For instance, an absolute difference of 0.01 in the surface albedo
351 leads to a change in AOD approximately by 0.1 and SSA by ~ 0.02 .

352

353 Figure 7 (top) shows the absolute difference in collocated SSA between OMI and SKYNET as a
354 function of concurrent SKYNET direct AOD (388 or 400 nm) measurements for all aerosol types.
355 All OMI-SKYNET matchup data obtained from a total of 25 sites under all AOD conditions are
356 included here. The data are shown in the box and whisker format, where the horizontal lines
357 represent the median value of each bin of sample size 150, filled circle the mean value, and
358 shaded vertical bars cover the 25 and 75 percentiles of the population in each data bin. While
359 for most bins the mean and median values of SSA difference were restricted to within ± 0.03 ,

360 OMI tends to overestimate SSA relative to that of SKYNET at lower AODs giving larger
361 differences and spread in the data population. Similar patterns were observed when the
362 difference in SSA was related to the OMI-retrieved AOD (Figure 7 middle). In both cases, the
363 differences in SSA minimize at larger AOD values (>0.5) suggesting a convergence in both
364 retrievals. Figure 7 (bottom) shows a similar plot of SSA difference against the concurrent OMI
365 UVAI. Notably, the differences in SSA exhibit even a stronger relationship to UVAI than that in
366 the AOD case (top and middle). For UVAI lesser than zero, the differences in the retrieval are
367 found to be beyond the expected uncertainty in both inversions, at least in the mean sense. For
368 the lower range of UVAI, OMI algorithm mostly employs the urban/industrial model for the
369 retrieval where all aerosols are assumed to be confined within the boundary layer (<2 km) with
370 a vertical profile that follows an exponential distribution. On the other hand, the mean and
371 median values of the SSA difference for UVAI larger than 0.2 for all bins fall within the 0.03
372 uncertainty range. The SSA differences approach to near-zero with a reduced spread at larger
373 magnitudes. Notably, both inversions are found to be in closer agreement for UVAI
374 measurements >0.3 .

375

376

377 **4 SOURCES OF UNCERTAINTY**

378 **4.1 UNCERTAINTIES IN THE GROUND-BASED SKYNET INVERSION PRODUCT**

379 The standard SKYNET inversion algorithm assumes a wavelength-independent surface albedo of
380 0.1 at all wavelengths across the UV to visible part of the spectrum. However, the algorithm
381 code allows flexibility to alter the value surface albedo in time and wavelength (Campanelli et
382 al., 2015). The diffuse light reflected from the ground plays a second-order role in the measured
383 sky radiances in most situations, however, has a potential to affect the SSA inversion, e.g.,
384 overestimated (underestimated) surface albedo can underestimate (overestimate) SSA
385 (*Dubovik et al.*, 2000; *Khatri et al.*, 2012). Using simultaneous inversion data from SKYNET and
386 AERONET for four representative sites, *Khatri et al.* (2016) have shown that the difference in

387 the prescribed surface albedo between SKYNET and AERONET results in a difference of ~ 0.04 in
388 SSA at red (675 nm) and near-IR wavelengths retrieved from the two collocated ground sensors.
389 The difference in SSA can also reach as large as ~ 0.08 when surface albedo differed by 0.3. The
390 assumed surface albedo value of 0.1 at near-UV (340 and 380 nm) and shorter visible
391 wavelength (400 nm) seems to be unrealistic for the vegetated and urban surfaces. The surface
392 albedo database at 354 nm and 388 nm derived from multiyear observations from OMI
393 suggests that the vegetated surfaces and urban centers are characterized with the lower values
394 of surface albedo, i.e., ~ 0.02 - 0.03 and ~ 0.05 , respectively; for desert surfaces, the albedo could
395 be as high as 0.08-0.10. Significant differences in the assumed surface albedo values between
396 OMI and SKYNET at shorter wavelengths could be one of the responsible factors for
397 discrepancies in SSA noted over several sites, particularly at lower aerosol loading when the
398 uncertainty in surface characterization can amplify error in the SSA inversion.

399

400 To further investigate this effect, the difference in SSA between OMI and SKYNET as a function
401 of the simultaneous difference in surface albedo is analyzed and shown in Figure 8 (top). The
402 data are presented in a standard box and whisker plot format. The analysis reveals a link
403 between differences in SSA and surface albedo, where increasing differences in SSA
404 (OMI>SKYNET) are associated with significant negative biases in surface albedo between OMI
405 and SKYNET. In other words, large overestimation in SKYNET surface albedo causes
406 underestimation of retrieved SSA, which is consistent with the findings of *Dubovik et al.* (2000)
407 and *Khatri et al.* (2012, 2016), thereby resulting in a substantial positive difference in SSA
408 between OMI and SKYNET. Recently, *Mok et al.* (2018) have shown that the use of AERONET
409 surface albedo dataset at 440 nm in the SKYNET algorithm for the S. Korea region produces SSA
410 values larger by ~ 0.01 at near-UV wavelengths. Notably, differences in SSA tend to be lower
411 when the differences in surface albedo are also minimal, such that the mean and median values
412 of those bins remain within the expected uncertainties of ± 0.03 in both retrievals. This result,
413 along with the previous findings cited above, convincingly points out that the SSA inversion
414 from ground-based sensors, especially at lower aerosol loadings, is likely susceptible to the
415 prescribed surface albedo. The assumption of a fixed value of spectral surface albedo of 0.1 in

416 the SKYNET algorithm appears to be inappropriate calling for a revision using more accurate
417 datasets of spectral reflectance or albedo such as from MODIS and OMI.

418

419 The dependence of SSA difference on the local hour of SKYNET measurements is quantified in
420 Figure 8 (bottom). The SKYNET dataset accessed from the data server at Chiba University
421 doesn't contain information on the solar zenith angle. However, the local time of
422 measurements reported in the data file for each station can serve a proxy for the solar zenith
423 angle. The OMI-SKYNET matchups exhibit a systematic dependency, where the differences
424 between the two datasets become relatively minimal when early morning and late afternoon
425 inversions of SKYNET associated with higher solar zenith angle are collocated with OMI
426 overpass time around 1:30 PM equator-crossing time. Owing to a longer atmospheric optical
427 path at higher solar zenith angle, thereby better aerosol absorption signal, the ground-based
428 aerosol inversions, such as from AERONET and SKYNET, are expected to be more reliable for sky
429 measurements carried out during early morning/late afternoon.

430

431 SKYNET inversion algorithm (Skyrad.pack Version 4.2 and version 5) assumes aerosols of
432 spherical shape regardless of the actual aerosol type observed in the scene. Following a
433 detailed analysis of the effect of non-sphericity of the particles on the difference between the
434 retrievals carried out assuming spherical and spheroidal size distribution, *Khatri et al.*, (2016)
435 concluded that the assumed shape of particles has a non-significant impact on the retrieved
436 SSA. Their study revealed SSA difference of ± 0.01 for measurements having a maximum
437 scattering angle $< 120^\circ$ and difference of up to ± 0.02 at scattering angle $> 120^\circ$, where the
438 difference in the phase function is significant between spherical and spheroidal size
439 distributions (*Torres et al.*, 2018). The OMI-SKYNET collocation procedure, as shown in Figure 4,
440 yields relatively fewer matchups that are identified as dust aerosol type according to the
441 OMAERUV aerosol type identification scheme. A majority of the collocated data points were
442 derived over the desert site of *Dunhuang* in China showing a reasonable agreement in SSA
443 between OMI and SKYNET for dust aerosols further supporting the findings of *Khatri et al.*

444 (2016) that the SSA retrievals are not significantly impacted by the assumption of the shape of
445 particles, i.e., spherical or spheroidal.

446

447 Apart from the algorithmic assumptions, the calibration constant used for sky radiances
448 measured by SKYNET instruments can be a potential source of errors in the inversion. *Khatri et*
449 *al.* (2016) suggests that the calibration constant for sky radiances determined from the disk
450 scan method using solar disk scan area of $1^\circ \times 1^\circ$ (*Boi et al.*, 1999) may be underestimated
451 resulting in overestimated sky radiance and thus relatively higher SSA. Some of the larger
452 differences between in SSA between OMI and SKYNET, where OMI underestimates SSA relative
453 to the SKYNET, can be attributed to the imperfect calibration applied to the SKYNET sensors.

454 **4.2 POSSIBLE SOURCES OF UNCERTAINTIES IN OMAERUV RETRIEVALS**

455 Like other satellite-based remote sensing algorithms, OMAERUV also relies on assumptions
456 about the atmospheric and surface properties for the retrieval of aerosol properties. The single
457 largest known source of error in the OMI retrievals is the subpixel cloud contamination within
458 the OMI footprint. Given the footprint of size $13 \times 24 \text{ km}^2$ for near-nadir pixels which intercept
459 an area of about 338 km^2 on the ground, the presence of subpixel clouds may not be avoided
460 entirely. Currently, the algorithm assigns quality flags to each pixel which carries information on
461 the quality of the retrieval depending upon the observed conditions (*Torres et al.*, 2013).
462 Aerosol retrieval with the quality flag '0' are considered to be the best in accuracy as this
463 category of flag scheme largely avoids cloud-contaminated pixels by choosing the appropriate
464 thresholds in reflectivity and UVAI measurements.

465

466 Over the desert regions, e.g., the *Dunhuang* SKYNET site in China, the frequency of occurrence
467 of clouds is expected to be minimal. Therefore, it is less likely that the SSA retrievals over these
468 sites are affected by cloud contamination. A reasonable agreement between the two retrieval
469 datasets (Figure 3) supports this assumption. The quality flag scheme, however, cannot entirely
470 rule out the presence of small levels of subpixel cloud contamination or the presence of thin

471 cirrus in the OMI footprint, which can cause overestimation in the retrieval of SSA, such as
472 noted over the SKYNET sites in *Kasuga, Etchujima, Seoul, Bologna, and Pune*. Largest
473 uncertainties observed over these sites are associated with the urban-industrial aerosol type,
474 possibly due to the fact that the AOD's for this aerosol type are the lowest in the analysis, and
475 therefore, subject to the less sensitivity to absorption and possibly more affected by sub-pixel
476 cloud contamination.

477

478 Another possible source of uncertainty can be the assumption of the aerosol layer height. The
479 climatology of aerosol layer height derived from CALIOP measurements adequately describes
480 the observed mean layer of carbonaceous and desert dust aerosols (*Torres et al., 2013*). It is
481 particularly robust over the arid and semiarid areas where large numbers of cloud-free
482 observations were used in the calculation. However, note that the temporal and spatial
483 coverage of CALIOP is limited to 16-day repeat cycle over the same location. Variations in the
484 aerosol layer height not observed by CALIOP, therefore, will be missed out in the derived
485 climatology and thus can be a source of uncertainty. Sensitivity analysis of the OMAERUV
486 retrievals suggests that an overestimation (underestimation) in the aerosol layer height results
487 in an overestimated (underestimated) SSA. This is because an increase (decrease) in the
488 assumed aerosol layer height from the actual one enhances (reduces) absorption in the
489 radiance look-up table (not in the actual TOA measurements), which the OMAERUV algorithm
490 compensates by retrieving lower (higher) AOD and higher (lower) SSA to match with the
491 observations.

492

493 The third source of uncertainty that can affect SSA retrieval is the accuracy of the prescribed
494 surface albedo. For the surface characterization, the OMAERUV algorithm use a near-UV
495 surface albedo database derived using the multiyear OMI reflectivity observations. The method
496 adopts a minimum reflectivity approach, ensuring minimal or no contamination from the
497 atmosphere, i.e., aerosols and clouds, in the measurements. Afterward, the minimum
498 reflectivity dataset derived from the OMI observations was adjusted in the temporal domain to

499 the seasonality of surface albedo retrieved in the visible wavelengths from MODIS. The dataset
500 contains surface albedo values at 354 and 388 nm at a grid resolution of $0.25^\circ \times 0.25^\circ$.
501 Compared to the previous OMAERUV dataset using TOMS-based surface albedo product at 1°
502 grid resolution, the new OMI-based dataset is expected to be more accurate to within 0.005 to
503 0.01 owing to its higher spatial resolution and the fact that it is contemporary to the OMI
504 operation. A sensitivity study of the OMAERUV retrievals to the change in surface albedo
505 described in *Jethva et al. (2014)* suggests that an increase in surface albedo by 0.01 in the near-
506 UV region over desert areas results in a decrease in the magnitude of retrieved SSA by ~ -0.02 .
507 The effect of uncertain surface albedo can be more pronounced at lower aerosol loading,
508 where the reduced signal from the atmosphere makes OMAERUV retrieval more susceptible to
509 the uncertainty in surface albedo.

510

511 The assumed aerosol microphysical and optical properties could be additional sources of
512 uncertainty. The particle size distributions assumed in the OMAERUV models are adopted from
513 long-term AERONET inversion statistics (*Dubovik et al., 2002*), representing areas influenced by
514 smoke, dust, and urban/industrial aerosols, and therefore are considered realistic
515 representations of the total atmospheric column. The carbonaceous smoke aerosols are
516 assumed to be spherical in shape with a bimodal log-normal size distribution and characterized
517 with a steep absorption gradient, such that the Absorption Angstrom Exponent (AAE) in the
518 near-UV lies in the range 2.5-3.0, to adequately represent the organics in the biomass burning
519 smoke particles (*Kirchstetter et al., 2004; Jethva and Torres, 2011*). The desert dust aerosol
520 model follows bimodal log-normal size distribution with particles comprised of randomly
521 oriented spheroids with an axis ratio (shape factor) distribution adopted from *Dubovik et al.*
522 (2006). The sensitivity study followed by an actual inversion of OMI data presented in Torres et
523 al. (2018) demonstrates that the change in dust particle shape from spherical to spheroidal
524 distribution improved the AOD retrievals significantly and brought the equivalence between the
525 retrievals over left and right sides of the OMI swath for the dust belt region of the tropical
526 Atlantic. The associated changes in SSA retrievals were noted within ± 0.01 and -0.02 for the
527 scattering angle up to 100° - 150° and $>160^\circ$, respectively. The OMAERUV version 1.8.9.1 data

528 product used in the present study adopts spheroidal dust model based on the work of Dubovik
529 et al. (2006) and Torres et al. (2018). The spectral dependence of the refractive index in the
530 near-UV assumed in the dust aerosol model is generally consistent with the in-situ laboratory
531 measurements (*Wagner et al.*, 2012). For instance, retrieval of AOD and SSA for carbonaceous
532 aerosols using the smoke model with AAE of 1.90 (10% relative spectral dependence in the
533 imaginary index between 354 and 388 nm) and 1.0 (no spectral dependence in the imaginary
534 index), instead of the standard AAE assumption of 2.7, results in a decrease in SSA up to -0.07,
535 respectively, suggesting a marked sensitivity of the SSA retrieval to the significant changes in
536 the spectral aerosol absorption. Due to the shortage of ground-based characterization of
537 absorption in the near-UV part of the spectrum, the regional representation of the spectral
538 absorption properties in the OMAERUV models is limited. Therefore, spatial and temporal
539 variations in the spectral properties of aerosols can be a potential source of error in the SSA
540 retrieval.

541

542 **5 SUMMARY AND CONCLUSION**

543 We presented a comparative analysis of the aerosol SSA retrieved from the OMI's two-channel
544 aerosol algorithm (OMAERUV) against an independent ground-based inversion made by the
545 SKYNET Sun photometers over selected 25 sites located mainly in Asia and Europe. This study
546 follows our previous efforts of evaluating the OMI near-UV SSA product carried out using
547 ground-based AERONET dataset (*Jethva et al.*, 2014). The capability of SKYNET sensors to
548 measure the Sun and sky radiance at near-UV wavelengths (340-380-400 nm), and
549 subsequently retrieve the aerosol optical properties, including SSA, at these wavelengths
550 provide a unique opportunity to directly compare the two near-UV SSA products from ground
551 and satellite. Ground-based inversion of SSA at the near-UV wavelengths eliminates the need to
552 adjust and extrapolate satellite retrieval to the visible wavelengths such as the case with
553 comparison against AERONET. Since the SSA inferred from two different platforms are
554 essentially retrieved from two fundamentally different inversion algorithms, the present study
555 does not stand as a "validation" exercise for either retrieval data sets. Instead, the purpose of

556 this analysis was to check the consistency (or lack thereof) between the two retrieved
557 quantities of the same physical parameter regarding standard statistical comparison, i.e., RMSD
558 and % of matchups within the expected uncertainties.

559

560 Unlike AERONET Level 2 inversion product that reports spectral SSA when AOD (440 nm)
561 exceeds a value of 0.4, SKYNET Level 2 dataset delivers spectral SSA in the near-UV and visible
562 parts of the spectrum under all cloud-free observations for all AOD conditions. The collocation
563 procedure that matched temporal inversion data from SKYNET with spatial retrievals from OMI
564 gave resulted in a total of 2691 collocated data points for AOD>0.0 and 1223 when AOD>0.3
565 collected from 25 sites representing biomass burning region of Southeast Asia, desert in China,
566 and urban/industrial areas in Japan, India, and Europe. Combinedly for all 25 sites and under all
567 AOD conditions, we find 38% and 59% of the total SKYNET-OMI SSA agree within their
568 estimated uncertainty range of ± 0.03 and ± 0.05 , respectively, with an overall root-mean-
569 square-difference of 0.06. When restricted with condition AOD>0.3 in both measurements, the
570 agreement of comparison improved to 51% and 72% with root-mean-square-difference of
571 0.047. When segregated by aerosol type, the agreement between the two sensors is found to
572 be robust for matchups identified as the carbonaceous aerosols over several sites in Japan,
573 *Seoul* in South Korea, *Phimai* in Thailand, and *New Delhi* in India, yielding 61% and 84% of data
574 points falling within the limits of ± 0.03 and ± 0.05 with an overall RMSD of 0.035. The
575 collocation procedure found few matchups for desert dust aerosol, mostly over *Dunhuang* site
576 in China, showing a reasonable comparison with 50% and 68% data points within expected
577 uncertainty limits. Among the three major aerosol types, the urban/industrial type aerosols
578 provide the maximum number of matchup data points with a relatively poorer comparison,
579 where 45% and 67% data are found to be within the uncertainty limits.

580

581 The differences in SSA between OMI and SKYNET are found to be larger at lower aerosol
582 loading, where OMI retrieves significantly higher SSA compared to that of SKYNET. However,
583 the differences are minimized at larger AOD values (>0.5) suggesting a convergence in both

584 retrievals at moderate to larger aerosol loading. Similarly, the differences in SSA exhibit a
585 stronger relationship to UVAI showing larger discrepancies beyond expected uncertainty limits
586 at lower UVAs (<0), but nearing to zero with a reduced spread in matchups at larger
587 magnitudes of UVAI (>0.2-0.3).

588

589 Much of the inconsistency observed between OMI and SKYNET at lower aerosol loading
590 indicates retrieval issues due to reduced signal-to-noise ratio and uncertain algorithmic
591 assumptions. For instance, the OMAERUV retrievals are more susceptible to the changes in
592 surface albedo at lower AODs, and to the spectral absorption at higher AODs (*Torres and Jethva,*
593 *2011*). On the other hand, the SKYNET inversion algorithm assumes a wavelength-independent
594 surface albedo of 0.1 across the UV to visible-near-IR wavelengths, which appears to be
595 unrealistic especially in the UV region where OMI surface albedo dataset shows much lower
596 values (<0.05) over land. Though the reflected light from surface plays a second-order role in
597 the ground-based retrievals, previous studies as well as results derived in the present work
598 (Figure 8) show that the uncertainty in surface albedo can cause non-negligible errors in SSA
599 retrievals that likely exceed the expected accuracy level of ± 0.03 .

600

601 Despite the inherent uncertainties associated with both satellite and ground inversion products,
602 a good level of agreement between the two independent techniques over SKYNET sites under
603 the favorable conditions, i.e., at higher aerosol loading, higher solar zenith angle, and when the
604 surface albedo assumption is consistent, is encouraging. We intend to extend the present
605 analysis to other SKYNET sites whose data are still not directly accessible in the public domain.
606 Continuing the evaluation of inversion products, both from satellite and ground, is an important
607 exercise to track the changes and improvements in the algorithms and resulting data products,
608 and to establish the consistency (or lack thereof) that can help to diagnose further and improve
609 the accuracy of retrievals.

610

611 **ACKNOWLEDGMENTS**

612 We thank the Center for Environmental Remote Sensing (CERes), Chiba University, Japan
613 (<http://atmos3.cr.chiba-u.jp/skynet/data.html>), for the online availability of the SKYNET dataset
614 for several sites in Japan, South Korea, China, India, Italy, and Germany. Acknowledgments are
615 also due to the principal investigators and their staff for establishing and maintaining respective
616 SKYNET sites, whose data are used in the present work. We acknowledge the support of NASA
617 GES-DISC, the NASA Earth Science data center, for the online availability of the OMI aerosol
618 product assessed in this analysis. Thanks are due to the two anonymous reviewers for offering
619 constructive comments leading to the improvements in the article.

620 AUTHORS' CONTRIBUTIONS

621 Dr. Jethva, the leading author, conceptualized the study and wrote the paper. He conducted
622 comparative data analysis of OMI- and SKYNET-retrieved single-scattering albedo products
623 presented in the paper. Dr. Torres (2nd author) brought his expertise in interpreting the results
624 and helped improving the manuscript writeup.

625

626 Additional Information

627 The author(s) declare no competing interests, financial or non-financial.

628 **REFERENCES**

-
- 629 Ahn, C., O. Torres, and P. K. Bhartia: Comparison of Ozone Monitoring Instrument UVAerosol
630 Products with Aqua/Moderate Resolution Imaging Spectroradiometer and Multiangle Imaging
631 Spectroradiometer observations in 2006, *J. Geophys. Res.*, 113, D16S27,
632 doi:10.1029/2007JD008832, 2008.
- 633
- 634 Ahn, C., O. Torres, and H. Jethva: Assessment of OMI near-UV aerosol optical depth over land, *J.*
635 *Geophys. Res. Atmos.*, 119, doi:10.1002/2013JD020188, 2014.
- 636
- 637 Boi, P., G. Tonna, G. Dalu, T. Nakajima, B. Olivieri, A. Pompei, M. Campanelli, and R. Rao:
638 Calibration and data elaboration procedure for sky irradiance measurements, *Appl. Opt.*, 38,
639 896-907, 1999.d
- 640
- 641 Campanelli, M., T. Nakajima, B. Olivieri: Determination of the solar calibration constant for a
642 sun-sky radiometer, *Applied Optics*, 43(3), 2004.
- 643
- 644 Campanelli, M., G. Gobbi, C. Tomasi, and T. Nakajima: Intercomparison between aerosol
645 characteristics retrieved simultaneously with a Cimel and Prede Sun-sky radiometers in Rome
646 (TorVergata AERONET site), *Opt. Pura Apl.*, 37, 3159–3164, 2004a.
- 647
- 648 Campanelli, M., V. Estelles, C. Tomasi, T. Nakajima, V. Malvestuto and J. A. Martinez-Lozan:
649 Application of the SKYRAD improved Langley plot method for the in situ calibration of CIMEL
650 sun-sky photometers, *Applied Optics*, 46(14), 2007.
- 651
- 652 Campanelli, M., Estellés, V., Colwell, S., Shanklin, J., and Ningombam S. S.: Analysis of aerosol
653 optical properties from continuous sun-sky radiometer measurements at Halley and Rothera,
654 Antarctica over seven years, *Geophysical Research Abstracts*, Vol. 17, EGU2015-2768, EGU
655 General Assembly, 2015.
- 656
- 657 Campanelli, M., A. M. Iannarelli, S. Kazadzis, N. Kouremeti, S. Vergari, V. Estelles, H. Diemoz, A.
658 di Sarra, A. Cede: The QUATRAM Campaign: QUALity and TRaceability of Atmospheric aerosol
659 Measurements, The 2018 WMO/CIMO Technical Conference on Meteorological and
660 Environmental Instruments and Methods of Observation (CIMO TECO-2018) “Towards fit-for-
661 purpose environmental measurements”, 2018.
- 662

- 663 Che, H., G. Shi, A. Uchiyama, A. Yamazaki, H. Chen, P. Goloub, and X. Zhang: Intercomparison
664 between aerosol optical properties by a PREDE skyradiometer and CIMEL sunphotometer over
665 Beijing, China, *Atmos. Chem. Phys.*, 8, 3199-3214, doi:10.5194/acp-8-3199-2008, 2008.
666
667
- 668 Dubovik, O., A. Smirnov, B. N. Holben, M. D. King, Y. J. Kaufman, T. F. Eck, and I. Slutsker,
669 Accuracy assessments of aerosol optical properties retrieved from Aerosol Robotic Network
670 (AERONET) Sun and sky radiance measurements, *J. Geophys. Res.*, 105(D8), 9791-9806,
671 doi:10.1029/2000JD900040, 2000.
672
- 673 Dubovik, O., B. N. Holben, T. F. Eck, A. Smirnov, Y. J. Kaufman, M. D. King, D. Tanre, and I.
674 Slutsker: Variability of absorption and optical properties of key aerosol types observed in
675 worldwide locations, *J. Atmos. Sci.*, 59, 590–608, 2002.
676
- 677 Dubovik, O., Sinyuk, A., Lapyonok, T., Holben, B. N., Mishchenko, M., Yang, P., Eck, T. F., Volten,
678 H., Munoz, O., Vehelmann, B., van der Zande, W. J., Leon, J. F., Sorokin, M., and Slutsker, I.:
679 Application of spheroid models to account for aerosol particle nonsphericity in remote sensing
680 of desert dust, *J. Geophys. Res.*, 111, D11208, <https://doi.org/10.1029/2005JD006619>, 2006.
681
- 682 Estellés, V., Campanelli, M., Smyth, T. J., Utrillas, M. P., and Martínez-Lozano, J. A.: Evaluation of
683 the new ESR network software for the retrieval of direct sun products from CIMEL CE318 and
684 PREDE POM01 sun-sky radiometers, *Atmos. Chem. Phys.*, 12, 11619-11630,
685 <https://doi.org/10.5194/acp-12-11619-2012>, 2012a.
686
- 687 Estellés, V., Campanelli, M., Utrillas, M. P., Expósito, F., and Martínez-Lozano, J. A.: Comparison
688 of AERONET and SKYRAD4.2 inversion products retrieved from a Cimel CE318 sunphotometer,
689 *Atmos. Meas. Tech.*, 5, 569-579, <https://doi.org/10.5194/amt-5-569-2012>, 2012b.
690
- 691 Estelles, V., N. Kouremeti, M. Campanelli, J. Grobner, J.A. Mari nez-Lozano, S. Kazadzis:
692 Preliminary aerosol optical depth comparison between ESR/SKYNET, AERONET and GAW
693 international networks. International SKYNET workshop, Rome (Italy), 2016.
694
- 695 Khatri, P., and T. Takamura: An algorithm to screen cloud affected data for sky radiometer data
696 analysis, *J. Meteor. Soc. Japan*, 87, 189-204, 2009.
697
- 698 Khatri, P., T. Takamura, A. Yamazaki, and Y. Kondo: Reterival of key aerosol optical parameters
699 for spectral direct and diffuse irradiances measured by a horizontal surface detector, *J. Atmos.*
700 *Oceanic Technol.*, 29, 683–696, 2012.

701
702 Khatri, P., T. Takamura, T. Nakajima, V. Estellés, H. Irie, H. Kuze, M. Campanelli, A. Sinyuk, S.-M.
703 Lee, B. J. Sohn, G. Pandithurai, S.-W. Kim, S. C. Yoon, J. A. Martinez-Lozano, M. Hashimoto, P. C.
704 S. Devara, and N. Manago: Factors for inconsistent aerosol single scattering albedo between
705 SKYNET and AERONET, *J. Geophys. Res. Atmos.*, 121, 1859-1877, doi:10.1002/2015JD023976,
706 2016.
707
708 Kirchstetter, T. W., T. Novakov, and P. V. Hobbs: Evidence that the spectral dependence of light
709 absorption by aerosols is affected by organic carbon, *J. Geophys. Res.*, 109, D21208,
710 doi:10.1029/2004JD004999, 2004.
711
712 Hansen, J., M. Sato, and R. Ruedy: Radiative forcing and climate response, *J. Geophys. Res.*,
713 102(D6), 6831-6864, doi:10.1029/96JD03436, 1997.
714
715
716 Hashimoto, M., Nakajima, T., Dubovik, O., Campanelli, M., Che, H., Khatri, P., Takamura, T., and
717 Pandithurai, G.: Development of a new data-processing method for SKYNET sky radiometer
718 observations, *Atmos. Meas. Tech.*, 5, 2723-2737, <https://doi.org/10.5194/amt-5-2723-2012>,
719 2012.
720
721 IPCC, 2013: Climate Change 2013: The Physical Science Basis. Contribution of Working Group I
722 to the Fifth Assessment Report of the Intergovernmental Panel on Climate Change (Stocker, T.F.,
723 D. Qin, G.-K. Plattner, M. Tignor, S.K. Allen, J. Boschung, A. Nauels, Y. Xia, V. Bex and P.M.
724 Midgley (eds.)). Cambridge University Press, Cambridge, United Kingdom and New York, NY,
725 USA, 1535 pp, doi:10.1017/CBO9781107415324.
726
727 Jethva, H., and O. Torres: Satellite-based evidence of wavelength-dependent aerosol absorption
728 in biomass burning smoke inferred from Ozone Monitoring Instrument, *Atmos. Chem. Phys.*, 11,
729 10,541–10,551, doi:10.5194/acp-11-10541-2011, 2011.
730
731 Jethva, H., O. Torres, and C. Ahn: Global assessment of OMI aerosol single-scattering albedo
732 using ground-based AERONET inversion, *J. Geophys. Res. Atmos.*, 119,
733 doi:10.1002/2014JD021672, 2014.
734
735 Mok, J., Krotkov, N. A., Torres, O., Jethva, H., Li, Z., Kim, J., Koo, J.-H., Go, S., Irie, H., Labow, G.,
736 Eck, T. F., Holben, B. N., Herman, J., Loughman, R. P., Spinei, E., Lee, S. S., Khatri, P., and
737 Campanelli, M.: Comparisons of spectral aerosol single scattering albedo in Seoul, South Korea,
738 *Atmos. Meas. Tech.*, 11, 2295-2311, <https://doi.org/10.5194/amt-11-2295-2018>, 2018.

- 739
740 Nakajima, T., G. Tonna, R. Rao, P. Boi, Y. Kaufman, and B. Holben: Use of sky brightness
741 measurements from ground for remote sensing of particulate polydispersions, *Appl. Opt.*, 35,
742 15, 2672-2686, 1996.
743
- 744 Schenkeveld, V. M. E., Jaross, G., Marchenko, S., Haffner, D., Kleipool, Q. L., Rozemeijer, N. C.,
745 Veefkind, J. P., and Levelt, P. F.: In-flight performance of the Ozone Monitoring Instrument,
746 *Atmos. Meas. Tech.*, 10, 1957–1986, <https://doi.org/10.5194/amt-10-1957-2017>, 2017.
747
- 748 Torres, O., P. K. Bhartia, J. R. Herman, Z. Ahmad, and J. Gleason: Derivation of aerosol
749 properties from satellite measurements of backscattered ultraviolet radiation: Theoretical basis,
750 *J. Geophys. Res.*, 103(D14), 17,099–17,110, doi:10.1029/98JD00900, 1998.
- 751 Torres, O., P. K. Bhartia, A. Sinyuk, E. J. Welton, and B. Holben: Total Ozone Mapping
752 Spectrometer measurements of aerosol absorption from space: Comparison to SAFARI 2000
753 ground-based observations, *J. Geophys. Res.*, 110, D10S18, doi:10.1029/2004JD004611, 2005
754
- 755 Torres, O., A. Tanskanen, B. Veihelmann, C. Ahn, R. Braak, P. K. Bhartia, P. Veefkind, and P.
756 Levelt: Aerosols and surface UV products from Ozone Monitoring Instrument observations: An
757 overview, *J. Geophys. Res.*, 112, D24S47, doi:10.1029/2007JD008809, 2007.
- 758 Torres, O., C. Ahn, and Z. Chen: Improvements to the OMI near-UV aerosol algorithm using A-
759 train CALIOP and AIRS observations, *Atmos. Meas. Tech.*, 6, 3257–3270, doi:10.5194/amt-6-
760 3257-2013, 2013.
- 761 Torres, O., Bhartia, P. K., Jethva, H., and Ahn, C.: Impact of the ozone monitoring instrument
762 row anomaly on the long-term record of aerosol products, *Atmos. Meas. Tech.*, 11, 2701-2715,
763 <https://doi.org/10.5194/amt-11-2701-2018>, 2018.
- 764 Wagner, R., T. Ajtai, K. Kandler, K. Lieke, C. Linke, T. Müller, M. Schnaiter, and M. Vragel:
765 Complex refractive indices of Saharan dust samples at visible and near UV wavelengths: A
766 laboratory study, *Atmos. Chem. Phys.*, 12, 2491–2512, doi:10.5194/acp-12-2491-2012, 2012.
767

768 TABLES

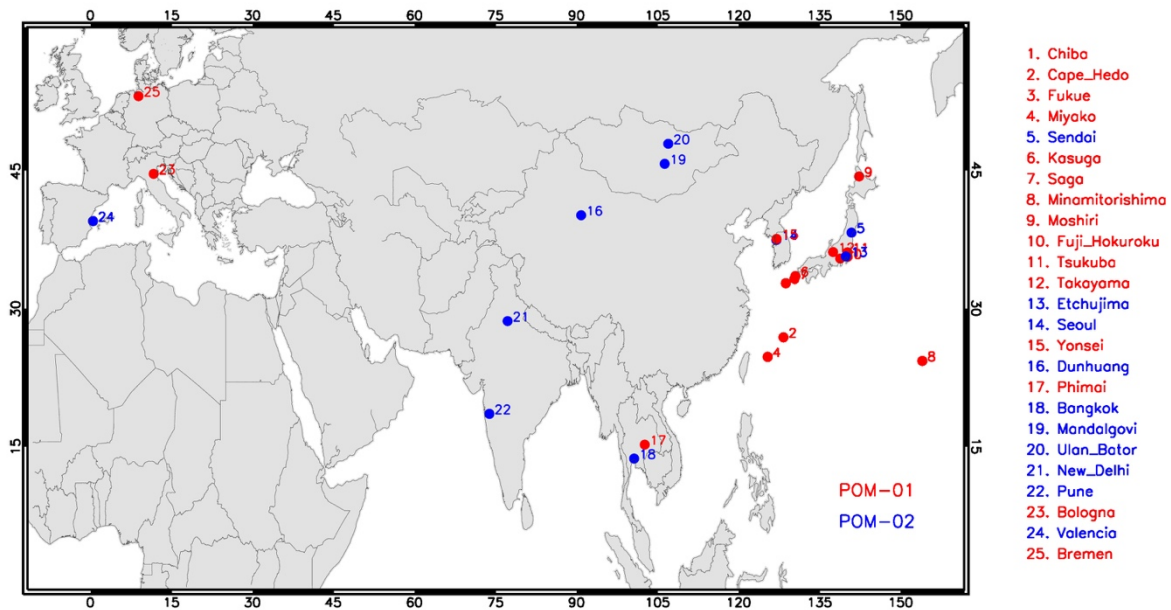
769 *Table 1 A list of SKYNET sites and corresponding dataset used in the present analysis. Sensor*
 770 *type “POM02” consists of a total of seven wavelength filters, including near-UV bands, i.e., 340,*
 771 *380, 400, 500, 675, 870, and 1020 nm, whereas “POM01” sensors have a total of five*
 772 *wavelength filters, i.e., 400, 500, 675, 870, and 1020 nm. The rightmost four columns enlist the*
 773 *statistical measures of OMI-SKYNET single-scattering albedo matchups.*

774 *Abbreviations: N: number of satellite-ground matchups, RMSD: root-mean-square-difference between OMI and*
 775 *SKYNET, Q_{0.03} and Q_{0.05}: percent matchups within an absolute difference of 0.03 and 0.05.*

SKYNET Station Name	Longitude	Latitude	Country	Sensor Type	Data Period	N	RMSD	Q _{0.03} (%)	Q _{0.05} (%)
<i>Chiba University</i>	140.104°E	35.625°N	Japan	POM02	2005-2017	132	0.039	58	81
<i>Cape Hedo</i>	128.248E	26.867N	Japan	POM02	2005-2017	47	0.044	47	72
<i>Fukue</i>	128.682E	32.752N	Japan	POM02	2008-2017	71	0.041	59	76
<i>Miyako</i>	125.327E	24.737N	Japan	POM02	2004-2017	31	0.059	23	58
<i>Sendai</i>	140.84E	38.26N	Japan	POM01	2009-2017	34	0.052	50	74
<i>Kasuga</i>	130.475E	33.524N	Japan	POM02	2004-2017	159	0.057	40	61
<i>Saga</i>	130.283E	33.233N	Japan	POM02	2011-2017	66	0.044	52	71
<i>Minamitorishima</i>	153.97E	24.3N	Japan	POM02	2006-2009	-	-	-	-
<i>Moshiri</i>	142.260E	44.366N	Japan	POM02	2009-2011	2	0.018	100	100
<i>Fuji Hokuroku</i>	138.750E	35.433N	Japan	POM02	2009-2017	9	0.051	56	67
<i>Tsukuba</i>	140.096E	36.114N	Japan	POM02	2014-2017	5	0.027	80	100
<i>Takayama</i>	137.423E	36.145N	Japan	POM02	2014-2017	3	0.022	67	100
<i>Etchujima</i>	139.796E	35.664N	Japan	POM01	2004-2010	100	0.052	45	66
<i>Seoul</i>	126.95E	37.46N	Republic of South Korea	POM01	2005-2015	182	0.050	42	66
<i>Yonsei</i>	126.980E	37.570N	Republic of South Korea	POM02	2016	5	0.035	40	80
<i>Dunhuang</i>	90.799E	40.146N	China	POM01	1999-2007	40	0.048	50	68
<i>Phimai</i>	102.564E	15.184N	Thailand	POM02	2005-2017	139	0.031	71	91
<i>Bangkok</i>	100.605E	13.667N	Thailand	POM02	2009-2017	15	0.064	47	60
<i>Mandalgovi</i>	106.264E	45.743N	Mongolia	POM01	1998-2009	4	0.087	0	0
<i>Ulan Bator</i>	106.921E	47.923N	Mongolia	POM01	2013-2017	2	0.026	100	100
<i>New Delhi</i>	77.174E	28.629N	India	POM01	2006-2007	63	0.038	52	83
<i>Pune</i>	73.805E	18.537N	India	POM01	2004-2009	94	0.050	39	64
<i>Bologna</i>	11.34E	44.52N	Italy	POM02	2014-2017	114	0.065	25	50
<i>Valencia</i>	0.420E	39.507N	Spain	POM01	2014-2017	4	0.052	25	25
<i>Bremen</i>	8.854E	3.108N	Germany	POM02	2009	-	-	-	-

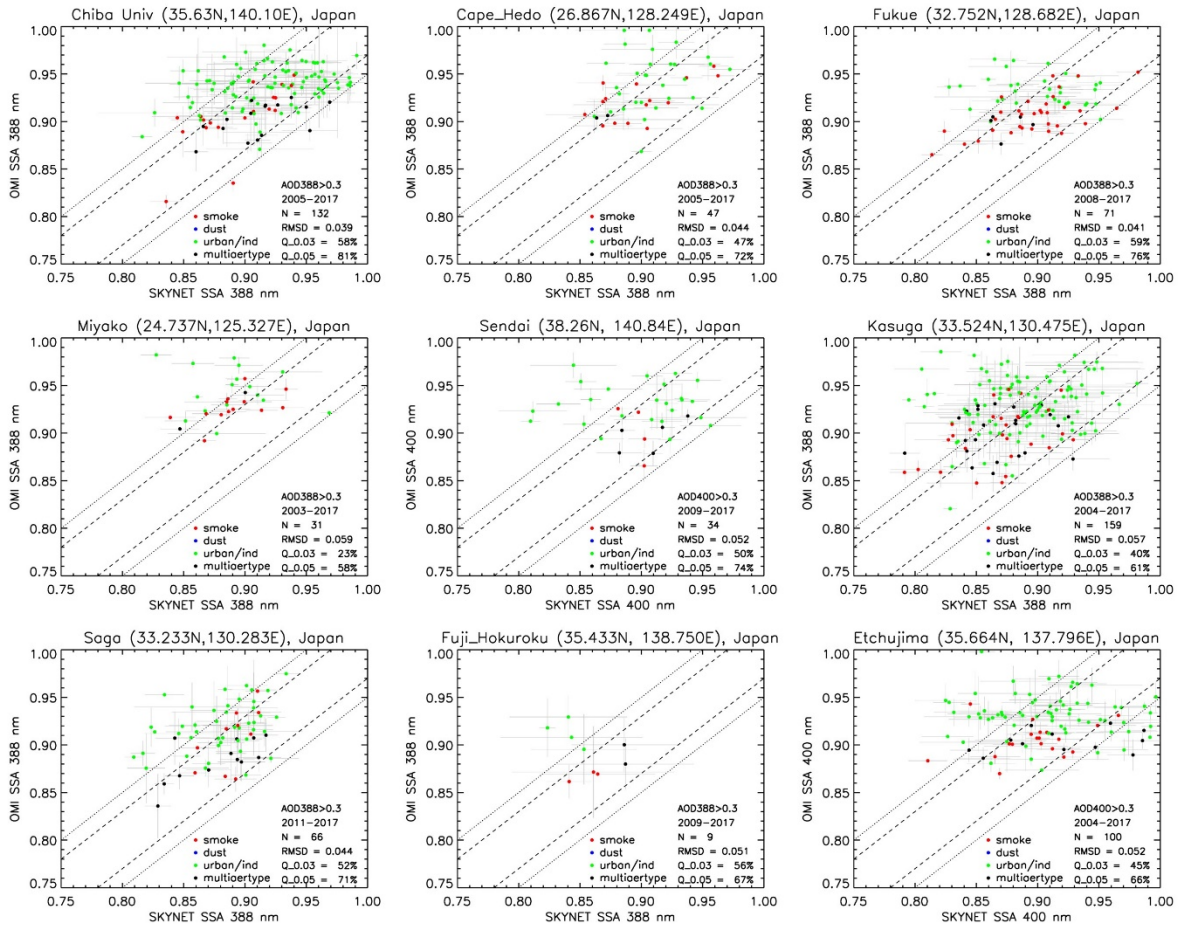
776

777 FIGURES



778

779 **Figure 1** Geographical placement of ground-based SKYNET sensors (POM-01 in blue, POM-02 in
 780 red) over sites in Asia and Europe The SKYNET dataset for these sites are freely accessible from
 781 the Center for Environmental Remote Sensing (CERes), Chiba University, Japan
 782 (<http://atmos3.cr.chiba-u.jp/skynet/data.html>).

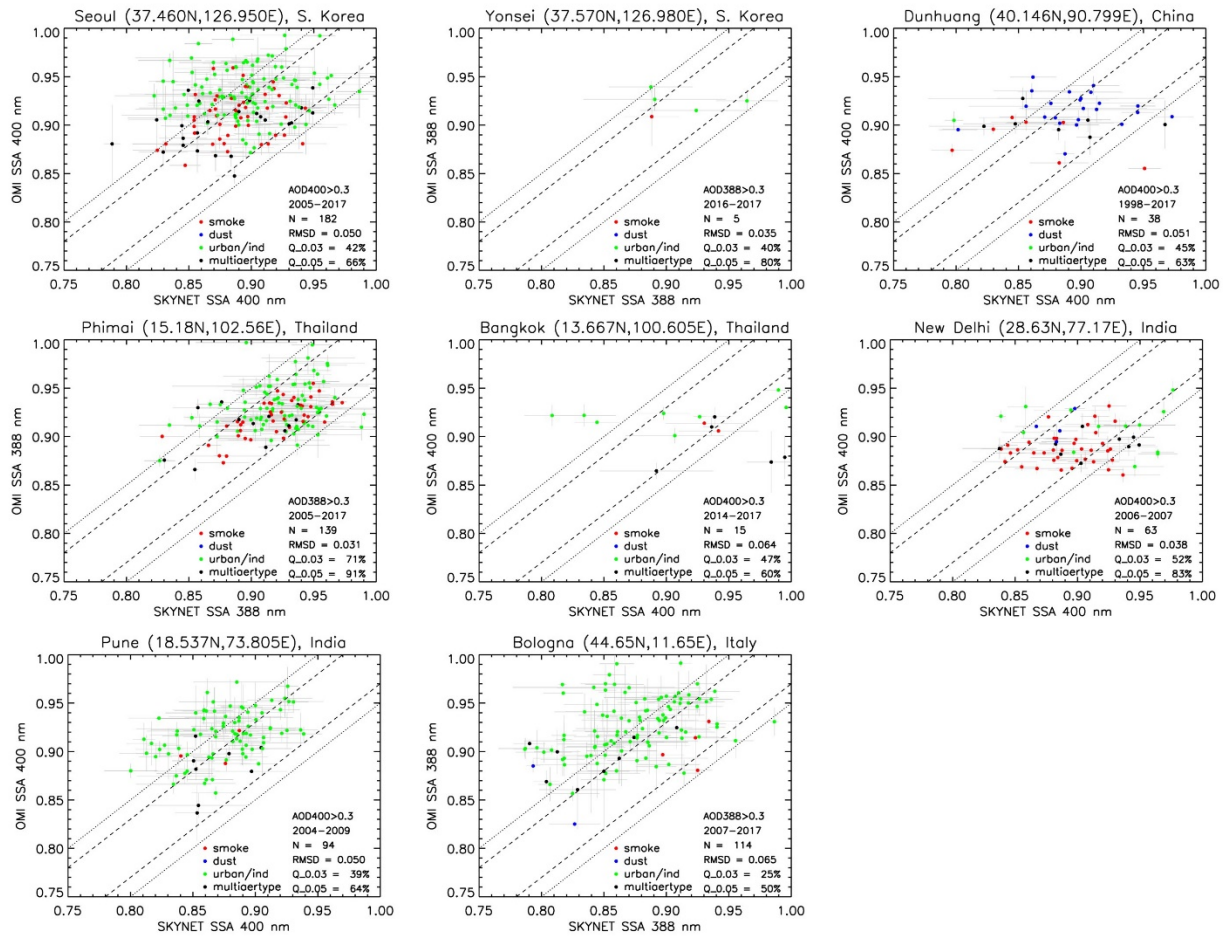


783

784 **Figure 2** OMAERUV versus SKYNET single-scattering albedo comparison for different sites in
 785 Japan. Legends with different colors represent the aerosol type selected by the OMAERUV
 786 algorithm for the co-located matchups (N). RMSD is the root-mean-square difference between
 787 the two retrievals; Q_{0.03} and Q_{0.05} are the percent of total matchups (N) that fall within the
 788 absolute difference of 0.03 and 0.05, respectively. OMI-SKYNET matchups with AOD>0.3 (388 or
 789 400 nm) in both measurements are used for comparison.

790

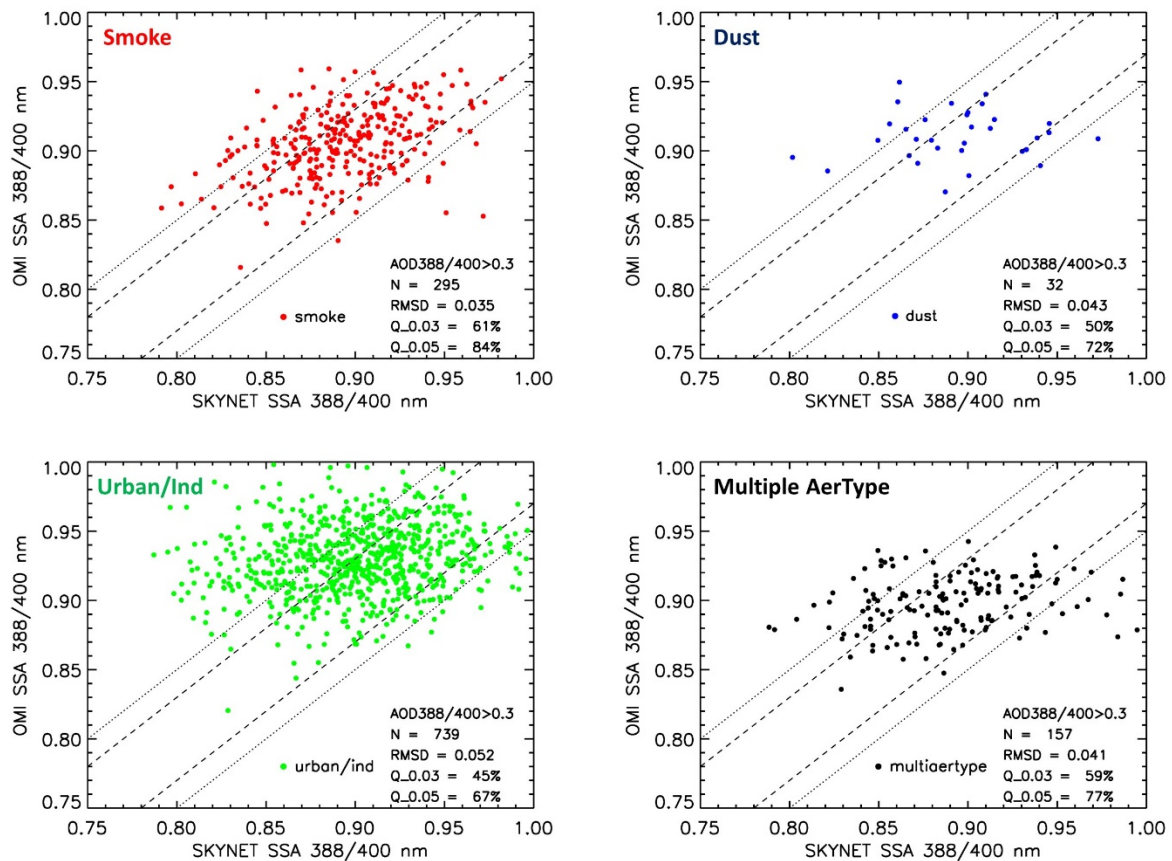
791



792

793 **Figure 3** Same as in Figure 2 but for SKYNET sites in South Korea, China, Thailand, India, and

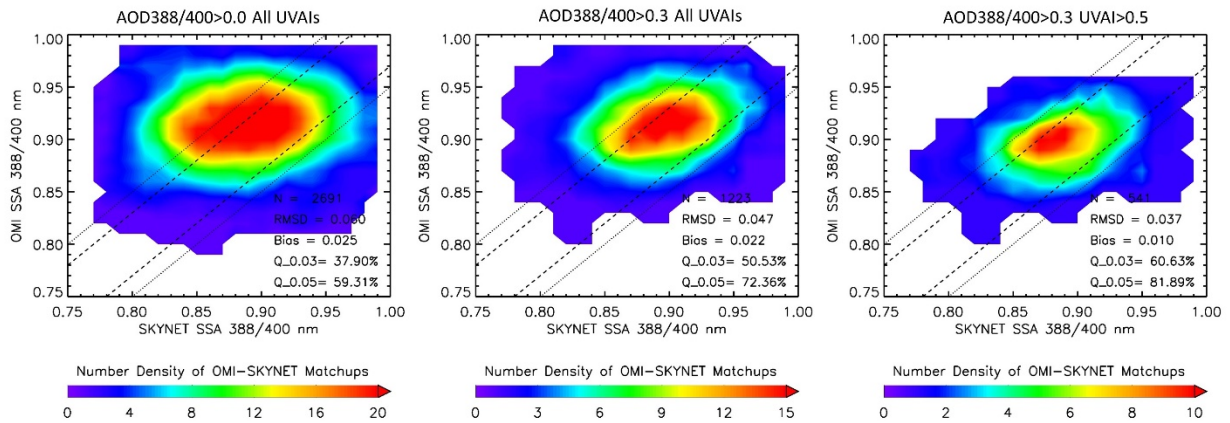
794 Italy.



795

796 **Figure 4** Composite scatterplots of OMAERUV versus SKYNET single-scattering albedo (388 or
 797 400 nm) for the three distinct aerosol types, i.e., smoke, dust, and urban/industrial, as
 798 identified by the OMAERUV algorithm. OMI-SKYNET matchups with AOD>0.3 (388 or 400 nm) in
 799 both measurements are used for the comparison.

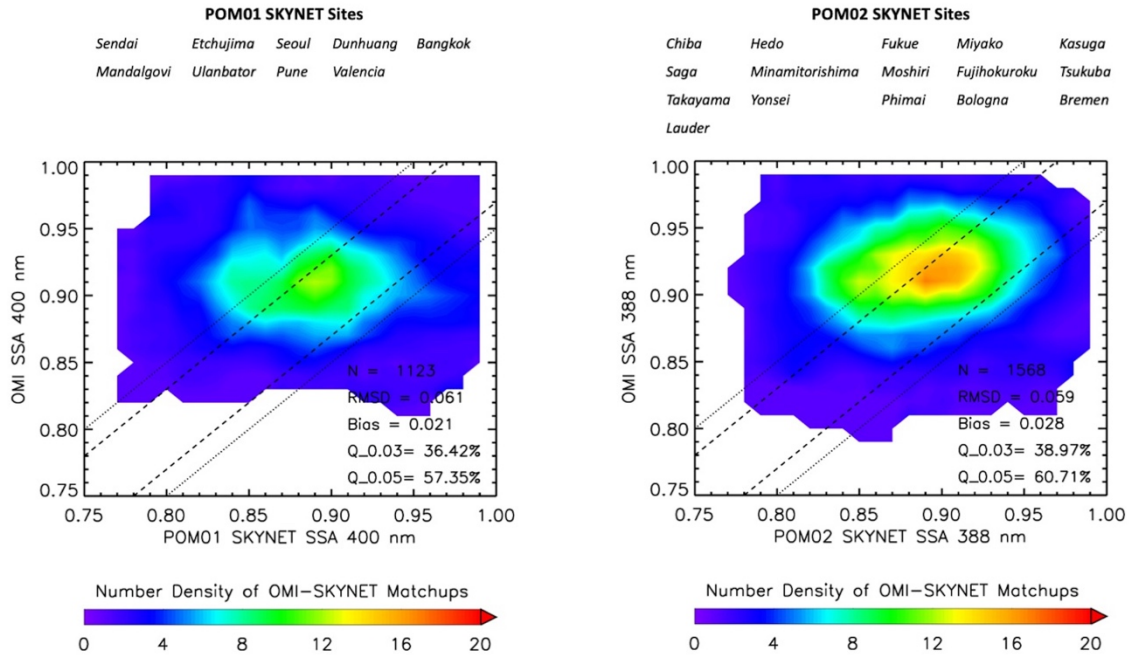
800



801

802 **Figure 5** Composite number density plots of SSA comparison between OMI and SKYNET for
 803 different aerosol loading conditions. The resultant statistics of the comparison are depicted in
 804 the lower-right in each plot. Note that the scale used for number density of satellite-ground
 805 matchups for the three sets of comparisons are different.

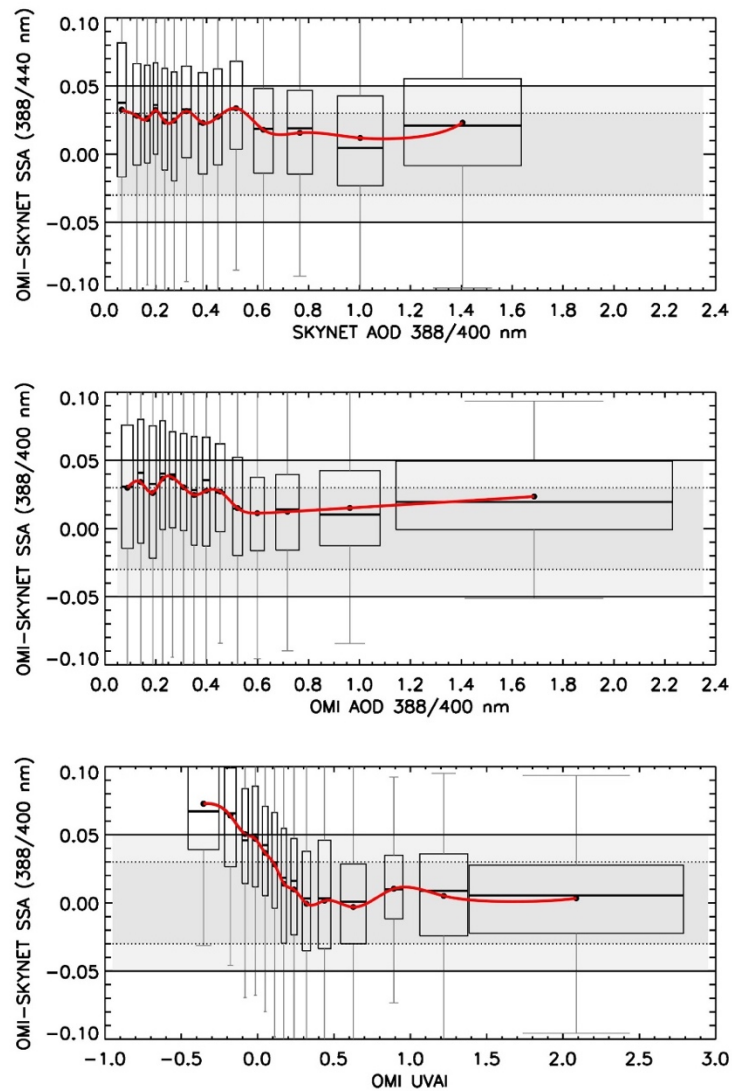
806



807

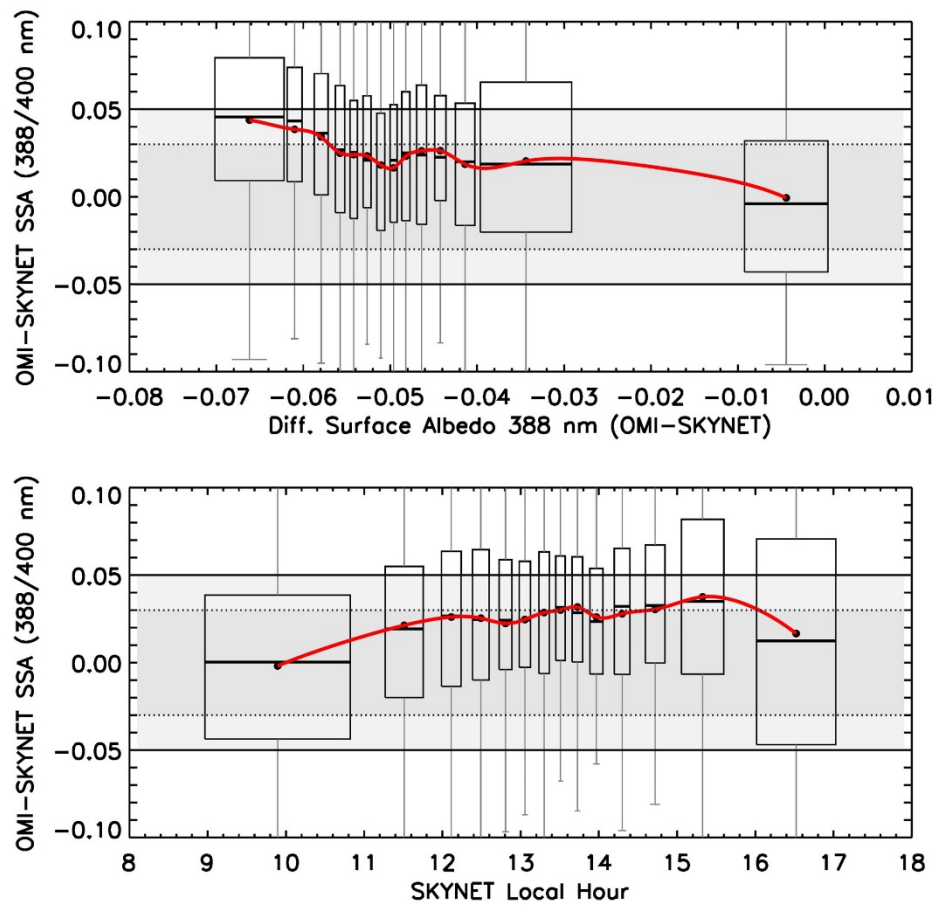
808 **Figure 6** Composite number density contour plots of SSA comparison between OMI and SKYNET
 809 for different aerosol loading conditions. The resultant statistics of the comparison are depicted
 810 in the lower-right in both plots.

811



812

813 **Figure 7** Difference in SSA between OMI and SKYNET as a function of the coincident SKYNET-
 814 measured (top panel) and OMI-retrieved (middle panel) aerosol optical depth and OMI-
 815 measured UVAI (bottom panel). Filled circles in black are the mean of difference for each AOD
 816 and UVAI bin with an equal sample size of 200 matchups; horizontal lines represent median of
 817 the bin samples; shaded area in gray encompasses data within 25 (lower) to 75 (higher)
 818 percentile range, whereas vertical lines in gray represent 1.5 times inter-quartile range (25 to
 819 75 percentile). The dotted and solid horizontal lines are the uncertainty range of ± 0.03 and
 820 ± 0.05 respectively. The width of each box represents 2-standard deviation of the data
 821 contained in the respective bins.



822

823 **Figure 8** Same as in Figure 7 but the difference in SSA between OMI and SKYNET is related to (a)

824 the difference in surface albedo assumed by the two algorithms and (b) local measurement

825 hour of SKYNET.